NJC

Accepted Manuscript

This article can be cited before page numbers have been issued, to do this please use: S. S, S. Soman, S. C. Pradhan, N. Unni, A. M. Peer, B. N. Nair and H. U. N. Saraswathy, *New J. Chem.*, 2016, DOI: 10.1039/C6NJ03098J.

View Article Online
DOI: 10.1039/C6NJ03098J

Journal Name

ARTICLE

Fine tuning compact ZnO blocking layers for enhanced photovoltaic performance in ZnO based DSSC: a detailed insight using β recombination, EIS, OCVD and IMVS techniques

Received 00th January 20xx,
Accepted 00th January 20xx

DOI: 10.1039/x0xx00000x

www.rsc.org/

Sasidharan Swetha,[a,b] Suraj Soman,[b,c]* Sourava Chandra Pradhan,[c] Narayanan Unni K. N,[b,c]* Abdul Azeez Peer Mohamed,[a] Balagopal Narayanan Nair[d,e] and Unnikrishnan Nair Saraswathy Hareesh[a,b]*

The electron-hole recombination and back electron flow at the conducting oxide-mesoporous film interface in Dye-Sensitized Solar Cells (DSSCs) are addressed primarily by the use of pre-blocking layers. Herein, the effects of zinc oxide (ZnO) blocking layers (BLs), on the photovoltaic performance of ZnO based DSSC are investigated in detail using electrochemical impedance spectroscopy (EIS), open circuit voltage decay (OCVD) and intensity modulated photovoltage spectroscopic (IMVS) techniques. BLs of varying thicknesses obtained by a low temperature solution process provided uniform surface coverage of nanosized ZnO particles over FTO. Devices with optimized ZnO blocking layer thickness (12 nm) lead to improved performance (efficiency 2.57%) in comparison to the devices fabricated using bare FTO (1.27%) by suppressing interfacial recombination at the FTO/ZnO interface thereby improving the lifetime leading to better performance.

1. Introduction

Dye-sensitized solar cells (DSSCs) are recognized as efficient, renewable and economic photovoltaic devices with potential for mass energy production.[1] In the past few years, concerted efforts are being pursued in the area of DSSC for the development of photoelectrodes using various functional materials.[2,3] The interface between conducting oxide and the functional layer plays a pivotal role in determining the charge dynamics of DSSCs particularly at low light conditions and hence is a crucial aspect for efficiency improvements.[4, 5] Titanium dioxide (TiO_2) is the most commonly used photoanode material in DSSCs, and to date the power conversion efficiencies (PCEs) up to 14% are realised with such devices.[6] Apart from TiO_2, zinc oxide (ZnO) is explored as a viable alternative in recent times due to its attributes like high bulk electron mobilities (1 order of magnitude higher than that of anatase TiO_2), wide band gap (3.37 eV) and large exciton binding energy (60 meV). Moreover, the ease of synthesising ZnO in a variety of architectures (ie; nanosheets,[7] nanowires,[8] nanotrees,[9] nanotubes,[10] nanotetrapods,[11] nanorods,[12] hierarchical aggregates[13] etc.) compared to TiO_2 also promotes the idea of titania substitution by ZnO .[2,14,15]

ZnO is considered to be the first semiconductor electrode to behave ideally in conjunction with a liquid electrolyte interface due to its low density of defects and potential distribution across the metal oxide/electrolyte interface.[16,17] However lower injection and electron transfer (ET) rate in ZnO based DSSC incite backward electron transfer processes (recombination) affecting the efficiency of devices.[18] Recombination of photoinjected electrons is one of the major limiting parameter in the performance of DSSCs which occurs either through recombination from FTO with the oxidized dye molecules or with the electrolyte at the FTO/electrolyte interface. Recombination also occurs from the bulk semiconductor material to the HOMO of the dye and also to the electrolyte.[19-22] This clearly necessitates the need to study the recombination process taking place on these devices in a more detailed fashion along with modifying the surfaces in a careful way to achieve higher efficiencies closer to that of TiO_2.

The present study addresses the former case as DSSCs find its primary application in devices that works in dim-light/indoor light conditions like decorations and sensors. Additionally Internet of Thing (IoT) supported applications are an emerging niche area for DSSC where it performs relatively better than its

[a] Materials Science and Technology Division, National Institute for Interdisciplinary Science and Technology (CSIR-NIIST), Thiruvananthapuram-695019, India.
[b] Academy of Scientific and Innovative Research (AcSIR), New Delhi, India.
[c] Photosciences and Photonics, Chemical Sciences and Technology Division, National Institute for Interdisciplinary Science and Technology (CSIR-NIIST), Thiruvananthapuram-695019, India.
[d] R&D Center, Noritake Co. Limited,300 Higashiyama, Miyoshi, Aichi 470-0293, Japan.
[e] Nanochemistry Research Institute, Department of Chemistry, Curtin University, GPO Box UI987, Perth, WA6845, Australia.

† Footnotes relating to the title and/or authors should appear here.
Electronic Supplementary Information (ESI) available: [details of any supplementary information available should be included here]. See DOI: 10.1039/x0xx00000x

View Article Online
DOI: 10.1039/C6NJ03098J

counterparts like c-Si and a-Si solar cells.[23-26] In DSSCs fabricated for these applications the recombination happening at FTO/electrolyte interface is more pronounced at the low light conditions as the total short circuit current is small. The recombination current from the FTO is also more important under low light intensity conditions, which necessitate the importance of having compact interlayers. At low light conditions the change in V_{oc} with light intensity is sharp due to the recombination at FTO/electrolyte interface.[27-30]

The widely adopted strategy to tackle this issue is to deposit blocking layers (BLs) over FTO/active layer interface. Studies revealed that incorporation of a blocking or barrier layer between FTO and mesoporous nanoparticle film can significantly reduce the back electron transfer thereby enhancing the PCE. The improved physical contact of metal oxide nanoparticles on the FTO surface suppresses the direct contact of FTO electrode with electrolyte thereby preventing recombination.[31-33] Several methods are available in the literature for the deposition of the BLs, which include spray pyrolysis,[4,33] sputtering,[30,31,34,35] atomic layer deposition,[36] thermal oxidation,[37] sol-gel methods,[38] electrochemical deposition[37] etc.

In the present work we study the effect of compact ZnO BLs, deposited using a simple low-temperature solution processing technique, on the recombination mechanism of ZnO based dye-sensitized solar cells. The thicknesses of the BLs were varied by using different concentrations of ZnO dispersions. The aim of the present study is to develop an in-depth understanding of the effect of back electron transfer at FTO/electrolyte interface in the presence and absence of compact ZnO blocking layers using small perturbation methods like electrochemical impedance spectroscopy (EIS), intensity modulated photovoltage spectroscopy (IMVS) and large perturbation open circuit voltage decay (OCVD) measurements.

It is well documented by Bisquert *et al.* that lifetime is a kinetic quantity that contains information not only on the rate constants of charge transfer taking place at the interface but also on the distribution of electronic states and electronic transition that intercede in the operation of DSSC.[39,40] With the right compact ZnO blocking layer with optimum thickness (12 nm), we have succeeded in getting longer lifetime and improved electron collection efficiency leading to higher J_{sc} and V_{oc} for better power conversion efficiencies.

2. Experimental

2.1 Deposition of blocking layer

ZnO nanoparticles were synthesised as per literature procedures.[41-43] About 2.95 g zinc acetate dihydrate (Merck) was dissolved in 125 ml methanol under stirring at 65 °C. A solution of 1.48 g of potassium hydroxide (HPLC pvt. Ltd.) in 65 ml of methanol was then added drop wise to the above solution at 60-65 °C with continuous stirring. This reaction mixture was stirred for 2.5 h at the same temperature. The ZnO nanoparticles formed were then allowed to precipitate for an additional 2 h at room temperature. These ZnO nanoparticles were then collected and washed with methanol. A dispersion of such particles is then made in a solvent mixture containing 70 ml, n-butanol, 5ml methanol, and 5ml chloroform to obtain a concentration of about 10 mg/ml. The thickness of the blocking layers was then adjusted by further dilution of the stock solution in n-butanol to obtain concentrations of 1, 2, 5 and 10 mg/ml of ZnO content solutions. These solutions were ultra sonicated and dip coated over cleaned FTO plates (Dyesol) to generate the blocking layers. These films were then annealed at 180 °C for 1 h in a laboratory oven prior to the deposition of the ZnO active layer. Blocking layers produced from the ZnO content 1, 2, 5 and 10 mg/ml are coded as BL1, BL2, BL3 and BL4 respectively.

2.2 ZnO Paste preparation for porous active layer

ZnO nanoparticles for the paste preparation were synthesized as mentioned above. 1.12 g of ZnO nanoparticles were made into a paste with 0.23 g of ethylcellulose (TCI) and terpeniol (TCI) in an agate.

2.3 ZnO Characterization

The crystal structure and phase determinations were performed using a X-ray diffractometer PANalytical X'Pert PRO operated with Cu Kα radiation (X-ray wavelength λ = 1.5406 Å). X-ray diffraction patterns (XRD) were collected in the 2θ range of 5 to 80°. Furthermore, the size and crystallanity of ZnO nanoparticles were investigated by high resolution transmission electron microscope (HRTEM, FEI Tecnai 30 G2S-TWIN) operated at an accelerating voltage of 300 kV. The morphology of the ZnO films was analysed by scanning electron microscope (SEM) JEOL JSM-5600LV. The samples were gold coated before imaging. AFM images (Tapping-mode) were recorded by using Bruker multimode 8 - AFM The thickness of blocking layers was measured using a Bruker Dektak XT profilometer. The surface area and pore size distribution of the ZnO particles and film were calculated from the adsorption/desorption isotherms of N_2 at 77 K by BET and BJH method using a Tristar II surface area and porosity analyser (Micromeritics instrument ,USA).

2.4 Fabrication and Characterization of DSSC

The FTO substrates used for ZnO deposition were systematically cleaned using detergent, distilled water, acetone and isopropanol. Deposition of blocking layers was carried out by dip coating technique. The deposited films were annealed at 180 °C for 1 h followed by deposition of active ZnO layer by doctor-blading. The electrodes were then put into programmed heating at 325 °C for 15 min, 375 °C for 15 min, 450 °C for 15 min, and 500 °C for 30 min and slowly cooled down to room temperature. Electrodes were then immersed into N719 dye solutions (0.3 mM) with CDCA as coadsorbent (10 mM) and kept at room temperature for 15 h. Counter

View Article Online
DOI: 10.1039/C6NJ03098J
Journal Name ARTICLE

electrodes were prepared by coating Pt paste (Dyesol) on FTO plates having pre-drilled holes and annealing at 380 °C for 20 min. The electrodes were then assembled with hot press using 25 µm surlyn spacer. The space in between both the electrodes were filled with liquid I^-/I_3^- electrolyte composed of the standard compositions of 1-butyl-3-methylimidazolium iodide, lithium iodide, iodine, guanidinium thiocyanate and 4-*tert*-butyl pyridine in acetonitrile. The drilled holes were sealed with microscopic cover slide and surlyn to avoid electrolyte leakage.

The photovoltaic performance of the fabricated DSSCs was measured using an AM 1.5 solar simulator (Newport Instruments, USA) equipped with a source meter (Keithley 2400) at room temperature. The IPCE measurement of the devices was performed under DC mode using a 250W xenon lamp coupled with Newport monochromator. The *J-V* properties of cells were measured using square shape mask with an active area of 0.25 cm^2 (without mask active area is 0.36 cm^2). The power of the simulated sunlight was calibrated by using a reference cell supplied by Newport instruments. Open circuit voltage (V_{oc}) decay measurements are done at open circuit. The cell was in the dark at the beginning of the measurement, and then the lights were turned on until the voltage got stabilized, followed by switching the light off and recording the decay of photovoltage. Lifetime data was transformed from the voltage decay part of the measurement through previously reported methods.[44, 45] The electrochemical impedance spectroscopy measurements of the devices were carried out using an Autolab PGSTAT302N equipped with FRA mode under forward bias in dark. The measurements were performed in a frequency range from 100 kHz to 0.1 Hz with logarithmically increasing order at an ac amplitude of 10 mV.[46] Intensity modulated photovoltage spectroscopy (IMVS) measurements were conducted using the same electrochemical workstation (Autolab PGSTAT302N) equipped with FRA and LED driver to drive the red LED (627 nm). Photovoltage response of the cells was analyzed in the frequency range of 1 Hz to 1 kHz. The amplitude of the sinusoidal modulation for IMVS measurements was 10% of the dc light.

3. Results and Discussion

3.1 Synthesis and characterization of ZnO nanoparticles and films

The ZnO nanoparticles for the fabrication of both blocking layers and active layer were synthesized by hydrolysis and condensation of zinc acetate dihydrate by potassium hydroxide in methanol at 60-65 °C according to the following equation.

$$\mathrm{Zn(CH_3COO)_2 + 2KOH \rightarrow ZnO + 2CH_3COOK + H_2O}$$

The resulting nanoparticles were about 5 nm in size and a stable dispersion of the same was prepared in a mixture of butanol, methanol and chloroform in order to fabricate the BL. Mesoporous ZnO active layer was fabricated by preparing ZnO nanoparticle paste and applied on BL deposited FTO glass by doctor blading technique. The thickness of the active layer was kept constant and the effect of back electron transfer at FTO/electrolyte interface was studied using ZnO blocking layers of varying thickness.

The XRD patterns of the as synthesised ZnO nanoparticles used for the fabrication of BL and the ZnO paste annealed at 500°C are shown in Fig. 1 (a) and (b) respectively. In both cases, diffraction peaks can be assigned to the ZnO having wurtzite structure matching with the JCPDS file no. 76-0704. The narrowing of the peaks after annealing is attributed to the increase in particle sizes. Fig. 2. (a and b) shows the TEM images of the dispersion of ZnO nanoparticle used for blocking layer deposition and paste preparation respectively. Fig. 2 (a) indicates that the particles posses an average diameter of 5 nm and SAED given in inset suggests high crystallinity of the ZnO nanoparticles. Fig. 2. (b) corresponds to the TEM of annealed ZnO paste used for active layer preparation, the average particle size was found to be increased to ~ 40 nm.

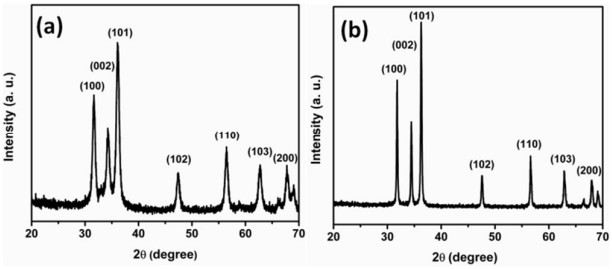

Fig. 1. a) XRD pattern of as synthesized ZnO nanoparticle b) XRD of ZnO film annealed at 500°C.

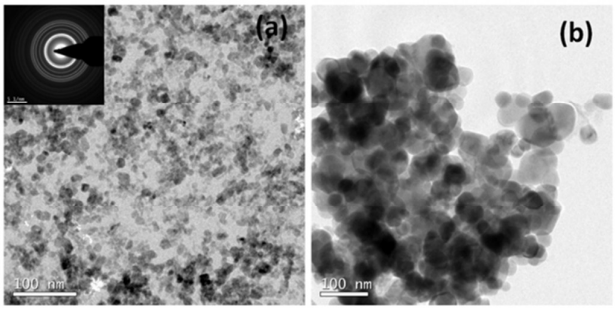

Fig. 2. TEM images of a) as-synthesized ZnO nanoparticles and b) its paste annealed at 500^{0}C.

Surface area and pore size distribution of the powder samples were measured using N_2 adsorption/desorption analysis at liquid N_2 temperature. ZnO nanoparticles showed Type II b isotherm with H3 hysteresis loop Fig. 3(a), which suggests that the particles form aggregates having non rigid slit shaped pores. BJH pore size analysis of the desorption isotherm is also shown in Fig. 3(b). This analysis revealed a pore size of ~8 nm. The surface area was calculated to be 37 m^2/g, its nitrogen adsorption-desorption isotherm are shown in Fig. 3(a). We

View Article Online
DOI: 10.1039/C6NJ03098J

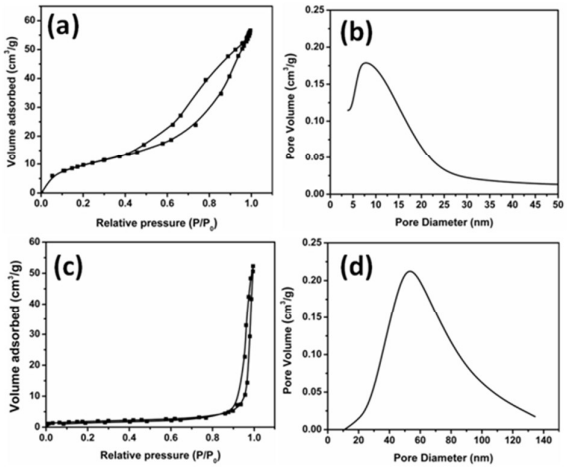

Fig. 3. N2 adsorption/desorption isotherms (a & c) and BJH pore size distribution curve (b & d) for as-synthesized ZnO nanoparticles and ZnO nanoparticles scraped from the annealed active layer.

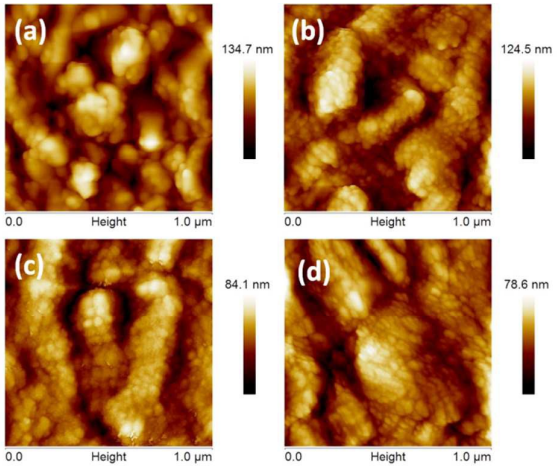

Fig. 4. AFM images of blocking layers coated on FTO glass a) BL1, b) BL2, c) BL3 and d) BL4.

have also analysed the surface area and pore size distribution of doctor bladed films using the same technique. ZnO film showed type II b isotherm with H3 hysteresis loop with a surface area of 6m^2/g (Fig. 3c). The BJH pore size distribution of the ZnO active layer (Fig. 3d) shows an average pore size of 53 nm, which is further supplemented by the SEM image presented in Fig. S1 (SI). Such kinds of films with high meso porosity are desirable for the adsorption of dye molecules.

Understanding the surface topography of blocking layers is critical for evaluating their suitability for photovoltaic applications. AFM analysis was employed to elucidate these features. AFM images shown in Fig. 4(a-d) provide the surface morphology of the BLs. The images suggest that the deposited ZnO layer provides much smoother surfaces as the concentration is increased, AFM image of the bare FTO substrate is presented in Fig. S2 (SI). The average thickness of the BLs were measured using profilometer and it was found to be 5±1 nm, 7±1 nm, 12±2 nm and 15±2 nm for BL1, BL2, BL3 and BL4 respectively.

Table 1. Concentration of ZnO solution and thickness of the blocking layers deposited.

Sample code	ZnO Concentration (mg/ml)	Thickness approx. (nm)
BL1	1	5 ±1
BL2	2	7 ±1
BL3	5	12 ±2
BL4	10	15 ±2

3.2 Photovoltaic characterization of dye-sensitized solar cells

3.2.1 current-voltage characteristics

The performance of all devices fabricated on bare FTO and FTO with ZnO pre-blocking layers of various thickness is tested under AM 1.5G irradiation (100 mW/cm^2). Fig. 5 (a) shows the photocurrent density-voltage characterization curves (*J–V*) for all the devices. Detailed photovoltaic performance parameters are listed in Table 2. The present work is more focused on to arrive at a simple method for the deposition of ZnO blocking layers and to understand its effect on the charge transfer and transport properties at the FTO/electrolyte interface using detailed small and large perturbation measurements. Hence the thickness of active ZnO layer was kept constant at ~20 µm in all cases. Devices fabricated on bare FTO exhibited short-circuit current density of (J_{SC}) of 3.95 mAcm^{-2}, open-circuit voltage (V_{OC}) of 0.61 V and fill factor (*FF*) of 0.53 respectively leading to an energy conversion efficiency of 1.27%. As the primary objective of the work was to elucidate the effects of ZnO blocking layers deposited by simple wet chemical deposition techniques on the interfacial charge transfer properties, further attempts were not made to achieve higher efficiencies. Compact ZnO pre-blocking layers were deposited on FTO substrates using simple dip coating method which resulted in layers with thickness 5±1 nm (BL1), 7±1 nm (BL2), 12±2 nm (BL3) and 15±2 nm (BL4). There is a systematic improvement in performance of DSSC devices by the application of compact ZnO blocking layers deposited on FTO. DSSC devices with a 12 nm thick ZnO layer showed the best performance, with a short-circuit current density (J_{SC}) of 7.13 mA/cm^2, an open-circuit voltage (V_{OC}) of 0.64 V, a fill factor (*FF*) of 0.56, and a consequent efficiency of 2.57% which is more than double the improvement in performance in comparison with the devices without blocking layers. However, with a further increase in the ZnO film thickness to 15 nm, the efficiency decreased to 2.37% which is mainly attributed to the decrease in current density and voltage. The improved performance with application of blocking layers is mainly attributed to the increase in current density, with the increase in thickness from 0 nm to 12 nm the photocurrent density got improved from 3.95 mAcm^{-2} to 7.13 mAcm^{-2}. It is to be noted that the enhancement in current compared to the improvement in voltage and fill factor is negligible. It has been well documented by Hamann *et al.* that for DSSCs the current density (Jsc) is determined by light harvesting efficiency (*LHE*),

View Article Online
DOI: 10.1039/C6NJ03098J

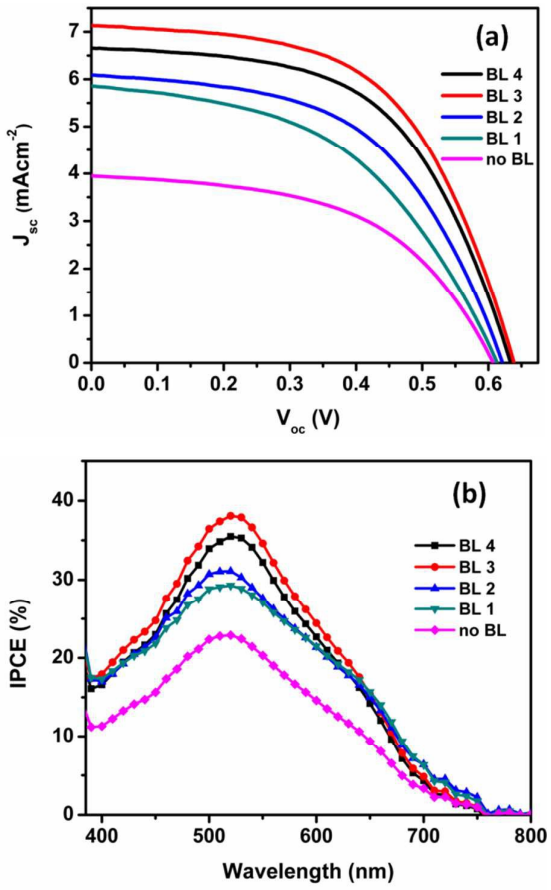

Fig. 5. (a) *J-V* and (b) IPCE characteristics without ZnO blocking layers and with blocking layers.

charge injection efficiency (η_{inj}), dye regeneration efficiency (η_{reg}) and charge collection efficiency (η_{cc}).[47,48] In the present work, we used the same dye (N719),electrolyte (I^-/I_3^-) and semiconductor active layer (ZnO) with similar thickness for fabrication of all devices. Thereby it is rational to assume similar LHE, η_{inj} and η_{reg} for all the devices under consideration. This clearly indicates that the enhancement in current density is mainly attributed to the improvement in charge collection efficiency which is directly influenced by the interfacial recombinations at FTO/electrolyte and ZnO/electrolyte interfaces. By employing compact blocking layers of ZnO on FTO, we were able to suppress the recombination taking place at the FTO/electrolyte interface. This results in more population of electrons in the conduction band of ZnO leading to a negative shift in quasi-Fermi level which impedes recombination enhancing current and voltage. Since both the blocking and active layers are made up of ZnO nanoparticle the charge generated at the conduction band is collected efficiently leading to an increased photocurrent density.

Table 2. Characteristic photovoltaic parameters obtained from DSSCs prepared with different ZnO compact blocking layers

Sample code	J_{sc} (mAcm^{-2})	V_{oc} (V)	*FF*	η (%)	R_S (Ω)	β	J_0 (mA)
no BL	3.95	0.61	0.53	1.27	52	0.57	4.1×10^{-6}
BL 1	5.86	0.61	0.49	1.75	41	0.63	1.7×10^{-6}
BL 2	6.09	0.62	0.53	2.02	34	0.64	9.7×10^{-7}
BL 3	7.13	0.64	0.56	2.57	30	0.70	1.5×10^{-7}
BL 4	6.66	0.63	0.56	2.37	28	0.64	7×10^{-7}

3.2.2 IPCE measurements

Fig. 5(b) represents the monochromatic incident photon-to-current conversion efficiency (IPCE) spectra of the fabricated DSSCs based on bare FTO and FTO/ZnO BL substrates with different ZnO BL thickness. The difference in short-circuit current density is entirely consistent with the trend obtained in IPCE measurements concerning equation 1 where e is the elementary charge, and $I_\circ(\lambda)$ is the solar irradiance spectra under AM1.5G condition.

$$Jsc = e \int I_\circ(\lambda) \times IPCE\ (\lambda) d\lambda \qquad (1)$$

Device fabricated on bare FTO gave an IPCE maximum of 22% whereas with the application of blocking layers with increased thickness the IPCE peak value and the characteristics in the visible region from 450-650 nm range got elevated systematically in the order of BL3 > BL4 > BL2 > BL1 > no BL reaching a maximum of 38% for devices fabricated with ZnO BL thickness of 12 nm. With further increase in thickness, the peak value got decreased to 36%. The IPCE results are in agreement with that of the *J-V* characteristics. As explained previously for current density, IPCE is related to light harvesting efficiency, injection efficiency, regeneration efficiency and charge collection efficiency by the equation

$$IPCE\ (\lambda) = LHE \times \eta_{inj} \times \eta_{reg} \times \eta_{cc} \qquad (2)$$

Considering the use of similar dye, electrolyte and ZnO paste with same thickness the net increase in the IPCE characteristic in the visible region can be attributed to better charge collection efficiency which was modulated in a meticulous way by careful tuning of compact ZnO blocking layers. In the case of TiO_2 based DSSCs the application of blocking layers leads to high series resistance in the cell. Thus employing TiO_2 BLs will prevent the back electron transfer from FTO to tri-iodide ions in the electrolyte under short circuit conditions whereas in open circuit conditions electrons used to accumulate at the surface of BLs resulting in high sheet resistance.[4,5,19] The effect of BLs in ZnO-based DSSC are entirely different where the presence of BLs leads to lowering of series resistance which is tracked using recombination parameter β. This is critical in the development of ZnO based DSSC.

View Article Online
DOI: 10.1039/C6NJ03098J

3.2.3 β recombination model analysis

To provide a deeper insight into the recombination mechanism taking place with and without the compact ZnO BLs, in the present ZnO based DSSC we used both the β recombination model and diode model employed for liquid electrolyte based DSSCs from Bisquert *et al.*[49,50] According to the conservation equation, the concentrations of electrons are determined using the equation,

$$\frac{dn}{dt} = G - U_n + U_{n0} \qquad (3)$$

where G denotes the charge carrier generated by the incident light given by the equation $G = \phi_{abs}/L$ where ϕ_{abs} is the photo flux and L being the thickness of the absorber layer. U_n is the recombination rate and U_{n0} is a term that gives equilibrium at $G = 0$. According to this model the recombination rate U_n is directly related to the n_c^{β} by the equation

$$U_n = k_{rec}\, n_c^{\beta} \qquad (4)$$

where n_c denotes free electrons located in conduction band, Fermi level and sub-band gap trap states, β is a constant parameter called recombination parameter which will have values $0 < \beta \leq 1$ in general for DSSC and k_{rec} is a recombination constant.[49-52]

At steady state the current density drawn from the solar cell, j can be determined by using equation (3) and (4) and integrating it over the entire active film thickness[49, 50] resulting in equation (5) given as

$$j = \emptyset_{abs} - qk_r n_C^B + qk_r n_0^B \qquad (5)$$

Equation (5) can be rewritten in the form of diode equation as

$$j = j_{sc} - j_0 \left(e^{q\beta V_F / k_B T} - 1\right) \qquad (6)$$

where j_{sc} is the short circuit photocurrent given by the equation $J_{sc} = q\phi_{abs}$ and j_0 determines the diode dark current as given in the Table 2, q is the charge of electron and V_F is the corrected voltage after subtracting the effect of series resistance as given by equation (7)

$$V_F = V_{app} - V_{series} \qquad (7)$$

V_{app} is the applied voltage during measurement and V_{series} is the voltage drop at the total series resistance given by equation (8).[53]

$$V_{series} = [j/(j_{sc} - j)] \int_{jsc}^{j} R_{series}\, dj \qquad (8)$$

The recombination parameter (β) is calculated by fitting the *J-V* data plot. In our case, the β values varied between 0.5 and 0.7. In general, it can be said that a higher β value will result in lower recombinations, thereby having a better lifetime leading to improved fill factor. In the present study the device devoid of BLs gave a β value of 0.57 and a dark current (J_0) value of 4.1×10^{-6} mA. The β value got increased up to 0.70 for BL3 leading to J_0 value of 1.5×10^{-7} and slightly decreased thereafter apparently suggesting that with the employment of compact ZnO BLs the improvement we observed with respect to the current density, V_{OC} and efficiency is primarily due to the prevention of recombination/back electron transfer at the FTO/electrolyte interface as been explained by Bisquert *et al.*[49,50]

It has to be also noted in particular that with the application of ZnO BLs we were able to achieve a considerable decrease in the series resistance (R_s) of the devices fabricated as given in Table 2. This could be because the presence of BLs helped in having better adhesion thereby reducing the R_s which resulted in lowering the dark current. It has been well documented that in the case of TiO_2 based DSSCs the presence of a compact nanostructured film on FTO helped in improving the adherence of active layer rather than on bare FTO.[54] In the present work compact ZnO blocking layers strengthen the mechanical stability of ZnO active layer which also translated into better reproducibility of the device fabrication and performance.

Fill Factor involves contributions from both series (R_{series}) and shunt resistances (R_{shunt}). In the present study we calculated the β recombination parameter by taking out the series resistance. Thereby the β values which are not exactly matching up with the *FF* as it contains only the shunt resistance. But it should also be taken into consideration that the trend obtained for β holds in good agreement with that of the *FF*.

3.2.4 EIS measurements

Electrochemical impedance spectroscopy (EIS) was carried out under different bias conditions in dark to probe the internal charge dynamics involving transfer and transport of electrons in operating devices leading to improved power conversion efficiencies. The impedance spectra were recorded at direct applied potentials from -0.3 V to -0.8 V, stepped in 0.1 V increments, with a 10 mV alternating potential superimposed on the direct bias. The ac modulation frequency was from 100 MHz to 100 kHz in logarithmically increasing order. Detailed fitting and interpretation of the obtained data was carried out based on the consolidated literature available in this area.[51,55]

The transport part was not visible in any of the Nyquist plots (Fig. S3, SI) which is a characteristic feature of ZnO based DSSC which is bestowed with higher charge transfer and transport leading to better charge collection efficiencies in comparison to TiO_2 active layers. It is important to note that since the transmission-line feature commonly attributed to electron transport in TiO_2 semiconductor oxides were not observed in the Nyquist plots of the ZnO devices (Fig. S3, SI) as documented previously by L. M. Peter *et al.*.[56] Reliable fitting of the data with transmission line model proposed by Bisquert *et al.*, [57] is therefore difficult to be applied in the present case and the Nyquist plots were fitted with R-RC-RC circuit

View Article Online
DOI: 10.1039/C6NJ03098J

(Randle's circuit, Fig. S4, SI) in the present case. The absence of transport feature reflects the higher mobility of electrons in ZnO compared to TiO_2. The interfacial charge recombination resistance (R_{ct}) and recombination lifetimes (τ_n) were obtained by fitting the experimental data and were plotted as a logarithmic function of the applied bias as given in Fig. 6(a) and 6(b). Both R_{ct} and τ_n are vital factors that provide better insight into the recombination pathways taking place at the FTO/electrolyte interface at short circuit conditions in DSSC.[58] Fig. 6(a) displays the variation of recombination resistance as a function of applied potential. It is quite clear from the graph that application of blocking layers resulted in improving the charge transfer resistance values in comparison to bare FTO which forbids the back electron transfer leading to better lifetime for the devices employing blocking layers as given in Fig. 6(b). The electron lifetime (τ_n) was calculated based on the formula $\tau_n = R_{ct} \times C_\mu$.[56]

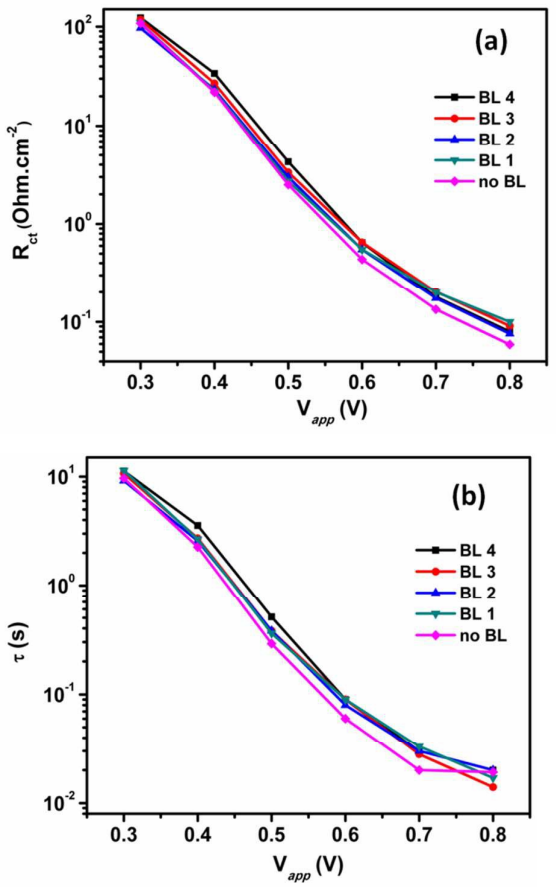

Fig. 6. (a) The variation of recombination resistance as a function of applied potential (b) variation of lifetime as a function of applied potential.

As reported previously by Vomiero *et al.* the variation of the trend in between the compact blocking layers on R_{ct} and τ_n are less pronounced for the data obtained from EIS measurements at short circuit conditions.[32] To gain a deeper understanding of the dynamics of electron transport taking place at the FTO/electrolyte interface we carried out detailed open circuit voltage decay measurements (OCVD) and intensity modulated photovoltage spectroscopic measurements (IMVS).

3.2.5 OCVD measurements

Open-circuit voltage decay (OCVD) is a powerful tool to study the recombination kinetics of photogenerated electrons with oxidized species in the electrolyte thereby providing information on the origin of the decrease in electron lifetimes.[40,45] OCVD technique involves turning off the illumination in a steady state and then monitoring the subsequent decay of photovoltage (V_{OC}). The lifetime / response time of the electron populated in conduction band and sub-band gap trap states are obtained by taking the reciprocal of the derivative of decay curve normalized by the thermal voltage as given by equation 9.

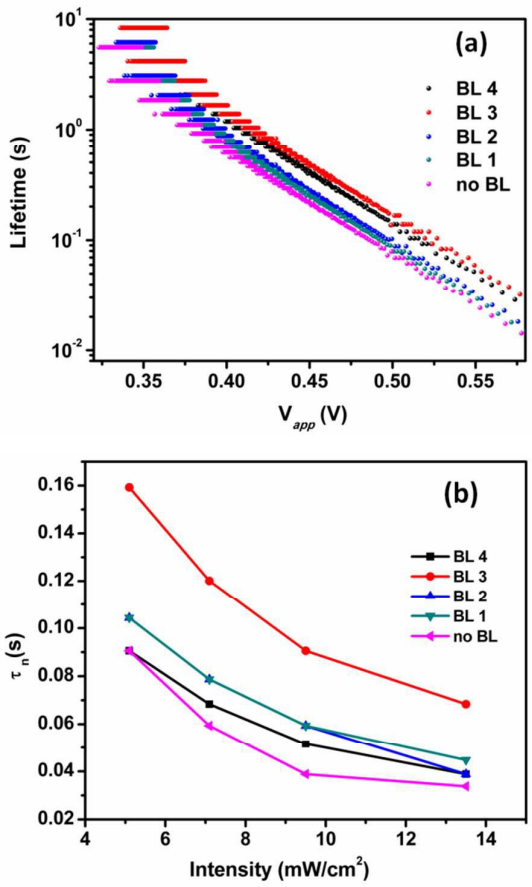

Fig. 7. (a) The variation of lifetime as a function of applied potential obtained from OCVD measurements (b) variation of lifetime as a function of light intensity obtained from IMVS measurement.

$$\tau_n = -\frac{k_B T}{e}\left(\frac{dV_{OC}}{dt}\right)^{-1} \quad (9)$$

View Article Online
DOI: 10.1039/C6NJ03098J

This method has an added advantage over the small perturbation techniques in both frequency and time domain (EIS, IMPS and IMVS) as OCVD gives a far better resolution along the Fermi level in one single and fast measurement.

In the present study, we aim to track the recombination taking place at the FTO/electrolyte interface where OCVD proves to be an excellent tool, the recombination of the photoinjected electrons with the oxidized dye cannot be measured by OCVD, as being a dark measurement. This helps in the interpretation of results in the present study and the trend in lifetime decay plots obtained by OCVD. Fig. 7(a) gives direct insight into the recombination taking place at the FTO/electrolyte interface. Fig. 7(a) shows the OCVD lifetime plots of devices fabricated on bare FTO and FTO with ZnO BLs of varying thickness. It is quite evident from the lifetime plot that with the application of ZnO BLs lifetime improved and the maximum was obtained for devices with a BL thickness of 12 nm (BL3). As the thickness further increased the lifetime decreased which could be due to the fact that with increased thickness the injection of electrons is blocked resulting in more recombination and reduction in lifetime. The lifetime was found to decrease in the order of BL3 > BL4 > BL2 > BL1 > no BL. The results pave light into the importance of studying recombination at the FTO/electrolyte interface which plays a significant role in determining the performance of the devices. The recombination kinetics can be modulated by the application of compact ZnO BLs on FTO substrates. The effect of compact BLs on solar cells performances is more pronounced at low light conditions where the total short circuit current is minimum. It has been documented that at lower intensities devices employing BLs gave a better open circuit voltage than that of the devices on bare FTO which finally translated to higher efficiencies.[30]

3.2.6 IMVS measurements

Charge transfer properties in nanostructured metal oxide films were studied using intensity-modulated photovoltage spectroscopy (IMVS) at various illumination intensities. A monochromatic red colour LED having a wavelength of 627 nm was used as the light source for illumination. The amplitude of the sinusoidal modulation for IMVS measurements was 10% of the dc light at a frequency range of 1 Hz to 1 kHz. The applied frequency was in logarithmically increasing order. It has to be noted that in DSSC the recombination can not only happen from the conduction band of ZnO but also from the sub-band gap trap states of both active layers and blocking layers.[59] The lifetime of electrons at different steady state can be determined more accurately by intensity modulated photovoltage spectroscopy (IMVS).[60,61] The lifetime so measured is strongly dependent on both Fermi level/open-circuit photovoltage V_{OC} and contains information not only on the rate constants of charge transfer but also on the distribution of electronic states and the transition taking place from them that intervene the normal forward electron transfer process in DSSC.[39] In the present work we carried out IMVS measurements at open circuit at a given steady state in a way to probe the recombination taking place from the conduction band. Since the switching frequency of the LED light (627 nm) is high the lifetime response involves both recombination to the electrolyte as well as to the dye ground state from ZnO conduction band. The electron lifetime (τ_n) is calculated from the IMVS measurement using equation 10,

$$\tau_n = \frac{1}{2\pi f_{IMVS}} \qquad (10)$$

where f_{IMVS} is the frequency at the top of the semicircle in the Nyquist plots or the peak frequency in the IMVS Bode plots. The corresponding lifetime at various illumination intensities is shown in fig. 7(b). The lifetime was found to decrease in the order BL3 > BL4 > BL2 > BL1 > no BL.

Fig. 7(b) gives the variation in lifetime as a function of LED light intensity measured using IMVS technique. It is quite clear from the graph that application of compact ZnO BLs resulted in improving the lifetime to a greater extent and the lifetime of the cells followed the trend $\tau_{no\ BL} < \tau_{BL1} < \tau_{BL2} < \tau_{BL4} < \tau_{BL3}$ clearly indicating a visible improvement in electron lifetime by the application of BLs resulting from a reduction in charge recombination. However, it has to be noted that when the thickness increases above 12 nm, there is a decrease in lifetime due to more recombination taking place as a result of limited injection by the formation of a potential barrier blocking effect as a result of increased thickness. The lifetime data obtained from IMVS measurements are in good agreement with the *J-V* parameters given in Table 2.

It has been well documented in literature by L. M. Peter that in open circuit condition under illumination the quasi-Fermi level of the TiO_2 nanocrystalline layer rises and since solid phases equilibrate, the BL Fermi level also rises along the former resulting in a Fermi level that is uniform for both BL and active TiO_2 layer leading to an increased population of electron density in the BLs which lead to more recombination rather than blocking the back electron transfer.[3,5,19] In this context the present work where we employed ZnO BLs, the inherent property of better charge collection and transport of ZnO nanoparticle prevented the accumulation of charge in the ZnO BLs which helped in successfully preventing the recombination resulting in improved lifetime and better charge collection efficiency leading to lower series resistance and better performance. Also need to be noted that the increased charge density at the BLs results in an increase in E_F of BL which couples up with the increase in E_F of ZnO thus improving V_{oc} but this effect is less pronounced compared to charge collection efficiency, so J_{SC} is increased better in comparison to V_{oc}.

Compact blocking layers play a crucial role in perovskite solar cells.[43,62] Recently it has been shown by Martinson *et al.* that a 12 nm thick TiO_2 film deposited using ALD as an efficient compact blocking layer for flexible and stable inverted perovskite halide devices.[63] The higher mobility of ZnO makes it a better candidate in comparison to TiO_2 for the electron

View Article Online
DOI: 10.1039/C6NJ03098J

selective contact in perovskite solar cells where compact BLs can be of great relevance.

4. Conclusion

We demonstrated that ultrathin layers of ZnO blocking layers (BLs) can successfully prevent the back electron transfer from FTO to the electrolyte in ZnO based DSSC aiding efficient collection of photoinjected electrons leading to better performance. A 12 nm thick ZnO layer obtained by a solution based coating technique proved to have the best lifetime by successful prevention of recombination as evident from EIS, OCVD and IMVS measurements leading to highest photovoltaic performance. This effect will be more pronounced when we move to low light conditions. This was also supported by the trend obtained for the recombination parameter (β) and the dark current (J_0) extracted by fitting the *J-V* data. Care need to be given in choosing the right thickness of BLs, as increased thickness can also obstruct injection leading to reduced performance. We are currently in the process of exploring the feasibility of these compact blocking layers in both flexible DSSC and perovskite solar cells.

Acknowledgements

The authors acknowledge the Council of Scientific and Industrial Research (CSIR), New Delhi, Government of India for providing research facilities and financial support (CSC0114). The authors also acknowledge MNRE for financial support under CSIR-TAPSUN and CSIR-M2D programmes. S.S. thank Department of Science and Technology, Government of India, for INSPIRE Faculty Award (IFA 13-CH-115). Authors also acknowledge Mr. Kiran Mohan for TEM, Mr. Aswin Maheswar for AFM and Mr. Rajeev V. R. for thickness measurements. S Swetha thanks University Grants Commission, Government of India for providing Senior Research Fellowship.

References

1 B. O'Regan and M. Gratzel, *Nature*, 1991, **353**, 737-740.
2 J. A. Anta, E. Guillén and R. Tena-Zaera, *J. Phys. Chem. C*, 2012, **116**, 11413-11425.
3 L. Peter, *Acc. Chem. Res.*, 2009, **42**, 1839-1847.
4 P. J. Cameron and L. M. Peter, *J. Phys. Chem. B*, 2003, **107**, 14394-14400.
5 P. J. Cameron and L. M. Peter, *J. Phys. Chem. B*, 2005, **109**, 7392-7398.
6 K. Kakiage, Y. Aoyama, T. Yano, K. Oya, J.-i. Fujisawa and M. Hanaya, *Chem Comm*, 2015, **51**, 15894-15897.
7 C.Y. Lin, Y.H. Lai, H.W. Chen, J. G. Chen, C.W. Kung, R. Vittal and K.-C. Ho, *Energy Environ Sci*, 2011, **4**, 3448-3455.
8 M. Law, L. E. Greene, J. C. Johnson, R. Saykally and P. Yang, *Nat. Mater.*, 2005, **4**, 455-459.
9 S. H. Ko, D. Lee, H. W. Kang, K. H. Nam, J. Y. Yeo, S. J. Hong, C. P. Grigoropoulos and H. J. Sung, *Nano Lett.*, 2011, **11**, 666-671.
10 A. B. F. Martinson, J. W. Elam, J. T. Hupp and M. J. Pellin, *Nano Lett.*, 2007, **7**, 2183-2187.
11 W. Chen, H. Zhang, I. M. Hsing and S. Yang, *Electrochem commun*, 2009, **11**, 1057-1060.
12 R. Gao, Z. Liang, J. Tian, Q. Zhang, L. Wang and G. Cao, *RSC Adv.*, 2013, **3**, 18537-18543.
13 N. Memarian, I. Concina, A. Braga, S. M. Rozati, A. Vomiero and G. Sberveglieri, *Angew. Chem., Int. Ed.*, 2011, **50**, 12321-12325.
14 W. Chen, Y. Qiu and S. Yang, *Phys Chem Chem Phys* , 2012, **14**, 10872-10881.
15 Y. He, J. Hu and Y. Xie, *Chem Comm*, 2015, **51**, 16229-16232.
16 A. Walker, H. J. Snaith, F. D. Angelis, E. D. Como, *Unconventional Thin Film Photovoltaics*, Royal Society of Chemistry, Cambridge, 2016.
17 J. F. Dewald, *J. Phys. Chem. Solids*, 1960, **14**, 155-161.
18 H. Wei, J.-W. Luo, S.-S. Li and L.-W. Wang, *J. Am. Chem. Soc.*, 2016, **138**, 8165-8174.
19 T. Oekermann, T. Yoshida, H. Minoura, K. G. U. Wijayantha and L. M. Peter, *J. Phys. Chem. B*, 2004, **108**, 8364-8370.
20 T. Oekermann, T. Yoshida, C. Boeckler, J. Caro and H. Minoura, *J. Phys. Chem. B*, 2005, **109**, 12560-12566.
21 E. Galoppini, J. Rochford, H. Chen, G. Saraf, Y. Lu, A. Hagfeldt and G. Boschloo, *J. Phys. Chem. B*, 2006, **110**, 16159-16161.
22 M. V. Vinayak, T. M. Lakshmykanth, M. Yoosuf, S. Soman and K. R. Gopidas, *Solar Energy*, 2016, **124**, 227-241.
23 T. Toyoda, T. Sano, J. Nakajima, S. Doi, S. Fukumoto, A. Ito, T. Tohyama, M. Yoshida, T. Kanagawa, T. Motohiro, T. Shiga, K. Higuchi, H. Tanaka, Y. Takeda, T. Fukano, N. Katoh, A. Takeichi, K. Takechi and M. Shiozawa, *J. Photochem. Photobiol. A*, 2004, **164**, 203-207.
24 C. L. Wang, P. T. Lin, Y. F. Wang, C. W. Chang, B.-Z. Lin, H. H. Kuo, C. W. Hsu, S.-H. Tu and C.-Y. Lin, *J. Phys. Chem. C*, 2015, **119**, 24282-24289.
25 Renewable energy focus.com, http://www.Renewable energyfocus.com/view/3304/can-dye-sensitised-solar-cells-deliver-low-cost-pv/, October 2008.
26 J. Eliasson , J. Delsing , S. J. Thompson , Y. -B. Cheng , and P. Chen, *Int. J. Ad. Syst. Meas.*, 2012, **5**(1&2), 45-54.
27 P. J. Cameron, L. M. Peter and S. Hore, *J. Phys. Chem. B*, 2005, **109**, 930-936.
28 S. Hore and R. Kern, *Appl. Phys. Lett.*, 2005, **87**, 263504.
29 A. Ofir, L. Grinis and A. Zaban, *J. Phys. Chem. C*, 2008, **112**, 2779-2783.
30 G. Pérez-Hernández, A. Vega-Poot, I. Pérez-Juárez, J. M. Camacho, O. Arés, V. Rejón, J. L. Peña and G. Oskam, *Sol. Energ. Mat. Sol. Cells*, 2012, **100**, 21-26.
31 M. S. Góes, E. Joanni, E. C. Muniz, R. Savu, T. R. Habeck, P. R. Bueno and F. Fabregat-Santiago, *J. Phys. Chem. C*, 2012, **116**, 12415-12421.
32 G. S. Selopal, N. Memarian, R. Milan, I. Concina, G. Sberveglieri and A. Vomiero, *ACS Appl. Mater. Interfaces*, 2014, **6**, 11236-11244.
33 L. Kavan and M. Grätzel, *Electrochim. Acta*, 1995, **40**, 643-652.
34 J. Xia, N. Masaki, K. Jiang and S. Yanagida, *J. Phys. Chem. B*, 2006, **110**, 25222-25228.
35 A. Alberti, G. Pellegrino, G. G. Condorelli, C. Bongiorno, S. Morita, A. La Magna and T. Miyasaka, *J. Phys. Chem. C*, 2014, **118**, 6576-6585.
36 J. Ding, Y. Li, H. Hu, L. Bai, S. Zhang and N. Yuan, *Nanoscale Res. Lett.*, 2013, **8**, 1-9.
37 L. Kavan, N. Tétreault, T. Moehl and M. Grätzel, *J. Phys. Chem. C*, 2014, **118**, 16408-16418.
38 J. Guan, J. Zhang, T. Yu, G. Xue, X. Yu, Z. Tang, Y. Wei, J. Yang, Z. Li and Z. Zou, *RSC Adv.*, 2012, **2**, 7708-7713.
39 J. Bisquert and V. S. Vikhrenko, *J. Phys. Chem. B*, 2004, **108**, 2313-2322.
40 J. Bisquert, A. Zaban, M. Greenshtein and I. Mora-Seró, *J. Am.* Chem. *Soc.*, 2004, **126**, 13550-13559.
41 C. Pacholski, A. Kornowski and H. Weller, *Angew. Chem. Int. Ed.*, 2002, **41**, 1188-1191.

View Article Online
DOI: 10.1039/C6NJ03098J

42 W. J. E. Beek, M. M. Wienk, M. Kemerink, X. Yang and R. A. J. Janssen, *The J. Phys. Chem. B*, 2005, **109**, 9505-9516.
43 D. Liu and T. L. Kelly, *Nat. Photon.*, 2014, **8**, 133-138.
44 S. Soman, Y. Xie and T. W. Hamann, *Polyhedron*, 2014, **82**, 139-147.
45 A. Zaban, M. Greenshtein and J. Bisquert, *ChemPhysChem*, 2003, **4**, 859-864.
46 S. Soman, M. A. Rahim, S. Lingamoorthy, C. H. Suresh and S. Das, *Phys Chem Chem Phys*, 2015, **17**, 23095-23103.
47 T. W. Hamann, R. A. Jensen, A. B. F. Martinson, H. Van Ryswyk and J. T. Hupp *Energy Environ Sci*, 2008, **1**, 66-78.
48 J. W. Ondersma and T. W. Hamann, *Coord. Chem. Rev.*, 2013, **257**, 1533-1543.
49 F. Fabregat-Santiago, G. Garcia-Belmonte, I. Mora-Sero and J. Bisquert, *Phys Chem Chem Phys*, 2011, **13**, 9083-9118.
50 K. Kalyanasundaram, *Dye-sensitized solar cells*, EPFL press, Lausanne, 2010.
51 J. Bisquert, F. Fabregat-Santiago, I. Mora-Seró, G. Garcia-Belmonte and S. Giménez, *J. Phys. Chem. C*, 2009, **113**, 17278-17290.
52 J. Bisquert and I. Mora-Seró, J. *Phys. Chem. Lett.*, 2010, **1**, 450-456.
53 F. Fabregat-Santiago, J. Bisquert, E. Palomares, L. Otero, D. Kuang, S. M. Zakeeruddin and M. Grätzel, *J. Phys. Chem. C*, 2007, **111**, 6550-6560.
54 K. Kalyanasundaram and M. Grätzel, Coord. Chem. Rev., 1998, **177**, 347-414.
55 J. Bisquert, D. Cahen, G. Hodes, S. Rühle and A. Zaban, *J. Phys. Chem. B*, 2004, **108**, 8106-8118.
56 E. Guillén, L. M. Peter and J. A. Anta, J. Phys. Chem. C, 2011, **115**, 22622-22632.
57 J. Bisquert, I. Mora-Sero and F. Fabregat-Santiago, *ChemElectroChem*, 2014, **1**, 289-296.
58 J. P. Gonzalez-Vazquez, G. Oskam and J. A. Anta, *J. Phys. Chem. C*, 2012, **116**, 22687-22697.
59 J. Bisquert, A. Zaban and P. Salvador, J. Phys. Chem. B, 2002, **106**, 8774-8782.
60 G. Schlichthörl, S. Y. Huang, J. Sprague and A. J. Frank, *J. Phys. Chem. B*, 1997, **101**, 8141-8155.
61 A. C. Fisher, L. M. Peter, E. A. Ponomarev, A. B. Walker and K. G. U. Wijayantha, *J. Phys. Chem. B*, 2000, **104**, 949-958.
62 B. E. Hardin, H. J. Snaith and M. D. McGehee, *Nat Photon*, 2012, **6**, 162-169.
63 I. S. Kim, R. T. Haasch, D. H. Cao, O. K. Farha, J. T. Hupp, M. G. Kanatzidis and A. B. F. Martinson, *ACS Appl. Mater. Interfaces,* 2016, **8**, 24310-24314.

View Article Online
DOI: 10.1039/C6NJ03098J

Table of contents

Fine tuning compact ZnO blocking layers for enhanced photovoltaic performance in ZnO based DSSC: a detailed insight using β recombination, EIS, OCVD and IMVS techniques

Sasidharan Swetha, [a,b] Suraj Soman,[b,c]* Sourava C. Pradhan,[c] Narayanan Unni K. N,[b,c]* Abdul Azeez Peer Mohamed,[a] Balagopal Narayanan Nair[d,e] and Unnikrishnan Nair Saraswathy Hareesh[a,b]*

[a]Materials Science and Technology Division, National Institute for Interdisciplinary Science and Technology (CSIR-NIIST), Thiruvananthapuram-695019, India.

[b]Academy of Scientific and Innovative Research (AcSIR), New Delhi, India.

[c]Photosciences and Photonics, Chemical Sciences and Technology Division, National Institute for Interdisciplinary Science and Technology (CSIR-NIIST), Thiruvananthapuram-695019, India.

[d]R&D Center, Noritake Co. Limited,300 Higashiyama, Miyoshi, Aichi 470-0293, Japan.

[e]Nanochemistry Research Institute , Department of Chemistry, Curtin University, GPO Box UI987, Perth, WA6845, Australia.

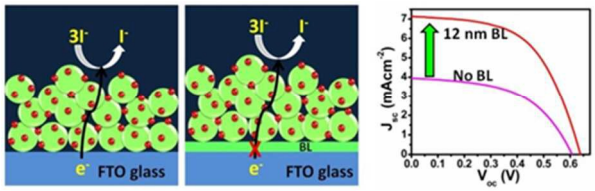

Exploitation of ultrathin ZnO blocking layers to prevent back electron recombination from FTO leading to enhanced photovoltaic performance.